GSA Data Repository item 2012328

Barnes et al. "Linking orography, climate, and exhumation across the central Andes"

Climate model and fission-track data, methods, and results

1. CLIMATE MODEL RESULTS

Rainfall estimates were extracted from the model simulations described in Insel et al. (2012), are reported in Table DR1, and plotted in Figure 2A in the main text. We chose REMOiso, because the model simulates reasonably well the modern precipitation gradient and estimates more accurate precipitation magnitudes along the Andes in comparison with other models. Insel et al. (2012) focuses on changes in $\delta^{18}O$ and isotopic lapse rates in response to Andean surface uplift. The paper shows surface uplift induced changes in precipitation on a continental scale to explain the simulated changes in the isotope values. In this paper, we present mean annual rainfall values from elevation scenarios (50-75-100% modern) along different Andean transects at the thrust belt scale. To compare our model results with geo-thermochronology data, we extracted the elevation and precipitation for each thrust belt zone in the different transects based on the mean values from ~4-6 model grid points (equivalent in size to the extent of each thrust belt zone).

2. FISSION-TRACK ANALYTICAL PROCEDURES

Mineral separations and fission track analyses (AFT for apatite, ZFT for zircon) were performed using standard techniques by Apatite to Zircon, Inc. (for details see the appendices in Donelick et al., 2005). Apatite grains were treated as described in Barnes et al. (2008). Zircon grains were mounted in FEP Teflon. Zircon mounts were also polished followed by immersion in a eutectic melt of NaOH + KOH at ~210(±10) °C for ~37 h and 10 min.

All zircon and most apatite analyses we report used the laser ablation (LA-ICPMS) method of Donelick et al. (2005). Age standards and zeta factor used are the same as in Barnes et al. (2008). Four apatite samples (AL1-2 and EC4-5) were analyzed with the external detector method (EDM) (e.g. Donelick et al., 2005). Age standards, zeta factor, and irradiation used are the same as in Barnes et al. (2006). The fission track data are reported in Table DR2 and sample locations and geologic context are shown in Figure DR1.

3. APATITE FISSION-TRACK ANALYSIS AND MODELING

We interpreted the apatite fission track data from sampled metasedimentary rocks using the same approach of Barnes et al. (2006; 2008), but with updated annealing models. We summarize only the updated part of the approach here.

We used HeFTy (v. 1.7.0) (Ehlers et al., 2005; Ketcham, 2005) to conduct sample thermal modeling. Input data for the inversions included the AFT grain ages, the AFT track-length distribution, and Dpar. We used the annealing model of Ketcham et al. (2007) with c-axis projected track lengths, the Cf irradiation option activated, and uncertainties at 95% +/-. We defined "good" and "acceptable" fits to the data estimated with a Kuiper's statistic after Ketcham (2005). The fission track data analyses are reported in Table DR3 with example thermal model results shown in Figure DR2.

4. EXHUMATION MAGNITUDE

We followed the procedures outlined in Barnes et al. (2006; 2008) to estimate exhumation magnitude and hence only describe the data relevant to the new FT data here.

Five proximal (within ~85 km) borehole measurements to our EC samples estimate a mean gradient of 23 ± 6ºC/km (stations Colquiri, Santa Fe, Huanuni, Bolivar, and Catavi (Henry and Pollack, 1988)). From this, we estimate an erosion magnitude of ~4.4 km and the range from 3.5-5.9 km for apatite and ~10 km with a range of 8-13 km for zircon (Fig. 2B). Estimated EC Oligocene paleo-geothermal gradients to the south are similar, ranging from 19-32ºC/km ± ~20% (Ege et al., 2007).

No thermal gradient measurements exist for the IA. Thus, we assume the gradient is the same as the EC at 23 ± 6ºC/km with equivalent estimated erosion magnitudes (Fig. 2B). An estimated IA Oligocene paleo-geothermal gradients to the south is very similar at 26ºC/km ± ~35% (Ege et al., 2007). Regional heat flow studies treat the IA as part of the EC further justifying the assumption of similar gradients between the EC and IA (Springer, 1999; Springer and Forster, 1998).

The new central SA sample cooling ages presented here are reset by the Miocene-to-recent deformation and/or orographically focused mean rainfall allowing us to estimate a depth to AFT closure as a minimum limit on SA exhumation. Over 1500 measurements from the southern Bolivia SA and adjacent Chaco plain yield a mean geothermal gradient of 22.4ºC/km ± ~35% (Springer and Forster, 1998). This gradient suggests the SA erosion magnitude is ~4 km (range ~3-6 km) or more. Unfortunately, no measurements exist proximal to these samples; hence this magnitude is the best estimate we can make with the geothermal data.

Table DR1. REMOiso mean rainfall estimates across the Bolivian orocline for 50%, 75%, and 100% modern elevations.

Region^	Mean Elev (m)*	Mean annual precipitation (m/yr)•		
		50% Elev	75% Elev	100% Elev
		north transect		
AL	3980	0.6	0.6	0.6
EC	3105	1.9	2.8	3.8
IA	1906	2	2.6	2.8
SA	1104	2	2.1	2
FL	371	2.4	2.3	2.1
		center transect		
AL	3871	1	1.1	1.1
EC	3252	1.2	1.6	2.4
IA	2036	1.5	2.2	3.9
SA	1073	1.6	2	2.9
FL	418	1.6	1.8	2.1
		south transect		
AL	3920	0.7	0.9	0.9
EC	3132	0.8	1.2	1.4
IA	1916	0.9	1.6	2.1
SA	996	0.7	1.2	1.3
FL	486	0.6	1	0.9

^region abbreviations same as in the text

*mean elevation of the region in the model at 100% modern elevation

•value reported is mean for 4-6 grid cells

Table DR2. Fission track data for the nort -central transect at the orocline apex. All samples are apatite except for EC7, which is paired with zircon (z).

Sample #	ID	Lat	Long	Elev m	Fm Age	n	Dpar µm	Dper µm	N_s trks	Area cm^2	∑(PΩ) cm^2	1σ ∑(PΩ) cm^2	ξ_{MS}	1σ ξ_{MS}	$P(\chi^2)$ %	Pooled Age Ma ± 2σ	MTL ± 1σ µm (N_t)
									Eastern Cordillera								
05JBBL070	EC1	-18.00	-66.95	3874	Sil	2	1.42	0.25	3	1.80E-05	1.10E-06	1.81E-07	12.983	0.2946	74.54	17.7 ± 21.2	13.63 ± 1.95 (5)
05JBBL071	EC2	-17.88	-67.02	3684	Sil	38	1.43	0.3	382	6.45E-04	7.78E-05	1.44E-06	16.4535	0.4781	49.12	40.3 ± 5.0	12.18 ± 2.64 (49)
05JBBL067	*EC3*	*-17.71*	*-66.66*	*3998*	*Sil*	*38*	*1.54*	*0.29*	*508*	8.88E-04	9.63E-05	1.67E-06	16.3686	0.4794	*0*	*43.0 ± 4.8*	11.59 ± 2.65 (38)
05JBBL065	*EC6*	*-17.66*	*-66.45*	*3559*	*Dv*	*39*	*1.51*	*0.29*	*814*	7.97E-04	9.25E-05	4.93E-06	13.0346	0.2957	*0.01*	*57.1 ± 7.8*	*12.57 ± 2.57 (193)*
05JBBL064	EC7	-17.66	-66.43	3209	Sil/Ord	37	1.48	0.27	94	4.89E-04	2.98E-05	1.94E-06	13.1328	0.298	6.1	20.7 ± 4.2	14.13 ± 1.72 (122)
05JBBL064z	EC7	-17.66	-66.43	3209	Sil/Ord	20	NA	NA	5450	1.45E-04	2.46E-05	4.43E-07	5.7138	0.2208	0	604 ± 56	NA
05JBBL062	*EC8*	*-17.60*	*-66.36*	*2761*	*Ord*	*5*	*1.43*	*0.28*	*10*	4.56E-05	1.13E-05	8.85E-07	16.4663	0.4779	*0*	*7.3 ± 4.8*	14.73 ± 1.07 (9)
									Interandean zone								
05JBBL060	IA1	-17.23	-65.89	3154	Ord	2	1.29	0.24	1	8.74E-06	1.53E-05	1.69E-06	16.4833	0.4777	92.06	0.5 ± 1.0	15.23 ± 2.63 (5)
05JBBL059	IA2	-17.17	-65.90	2772	Ord	19	1.69	0.41	7	2.02E-04	3.64E-07	4.66E-08	13.2064	0.2996	84.65	126 ± 100	10.45 ± 2.39 (90)
05JBBL058	*IA3*	*-17.19*	*-65.82*	*1787*	*Sil/Ord*	*27*	*1.39*	*0.24*	*21*	*2.07E-04*	*2.16E-05*	*7.29E-07*	*16.5618*	*0.4765*	*0*	*8.1 ± 3.6*	*14.03 ± 1.81 (28)*
									Subandes								
05JBBL056	SA1	-17.16	-65.74	1762	Ord	32	1.33	0.24	30	2.58E-04	4.49E-05	1.37E-06	16.7211	0.4741	65.13	5.6 ± 2.0	14.16 ± 1.54 (40)
05JBBL055	SA2	-17.10	-65.68	882	Ord	34	1.44	0.24	39	2.57E-04	7.95E-05	1.95E-06	16.891	0.4716	35.54	4.1 ± 1.4	14.22 ± 1.41 (33)
05JBBL054	SA3	-17.06	-65.65	611	Camb	14	1.53	0.34	2	4.80E-04	7.51E-06	9.36E-07	13.2616	0.3009	100	1.8 ± 2.6	14.27 ± 1.2 (23)
05JBBL052	*SA4*	*-17.02*	*-65.55*	*410*	*Sil/Ord*	*30*	*1.43*	*0.27*	*21*	2.67E-04	5.93E-05	1.19E-06	17.0609	0.4691	*0.02*	*3.0 ± 1.4*	14.15 ± 1.12 (44)

Sample #	ID	Lat	Long	Elev m	Fm Age	n	Dpar µm	Dper µm	N_s trks	ρ_s 10^6 t/cm^{-2}	ρ_i 10^6 t/cm^{-2}	N_i trks	ρ_d 10^6 t/cm^{-2}	N_d trks	$P(\chi^2)$ %	Pooled Age Ma ± 2σ	MTL ± 1σ (N_t) µm (trks)	C. Ages (N_g) Ma (N_g)
										Altiplano								
B815-5	*AL1*	*-18.49*	*-68.67*	*3950*	*Camb*	*13*	*1.76*	*0.46*	*93*	*0.045*	*1.319*	*265*	*4.208*	*4040*	*0.1*	*83.5 ± 20.8*	*12.03 ± 2.26 (51)*	31(4), 121(9)
B815-1	AL2	-18.48	-68.67	4144	Camb	24	1.62	0.44	49	0.045	0.251	271	4.217	4040	59.2	43.2 ± 13.6	12.43 ± 2.16 (100)	NA
										Eastern Cordillera								
B611-5	*EC4*	*-17.72*	*-66.61*	*3850*	*Dv*	*37*	*1.77*	*0.44*	*308*	*0.667*	*2.342*	*1082*	*4.275*	*4040*	*0*	*68.9 ± 9.8*	*11.9 ± 2.11 (201)*	51(29), 289(8)
66-7	EC5	-17.69	-66.51	3600	Ord	31	1.68	0.48	124	0.269	2.336	1078	4.283	4040	59.8	28.0 ± 5.6	12.59 ± 1.79 (121)	NA

SA = Subandes; IA = Interandean zone; EC = Eastern Cordillera; AL = Altiplano; Elev = Elevation; Fm age = Formation age; Cb = Carboniferous, Ord = Ordovician, Sil = Silurian, Dv = Devonian; Jr = Jurassic; K = Cretaceous; Camb = Cambrian; n = # of grains measured; Dpar = mean maximum diameter of fission-track etch figures parallel to c-axis; Dper = mean diameter perpendicular to c-axis; Ns = # of spontaneous tracks (trks) counted; Area = grain area analyzed; Σ(PΩ) = area weighted $^{238}U/^{43}Ca$, summed over n grains in sample; σ = standard deviation; ξMS = mass spectrometer zeta calibration factor; P(χ2) = probability (%) of greater chi- squared, failed samples (P(χ2)< 5) in italics; MTL = mean track length; N_t = number of track lengths measured; C. Ages = component ages deconvolved with BinomFit; Ng = number of grains in c. age; NA = not applicable

Table DR3. Summary of essential AFT data and HeFTy thermal modeling results

Sample #	ID	n	Dpar µm	Dper µm	P(χ^2) %	Pooled Age Ma ± 2σ	MTL ± 1σ µm (N_t)	Onset rapid cooling acceptable fits (Ma)	Onset rapid cooling good fits (Ma)	Data quality
							Eastern Cordillera			
05JBBL070	EC1	2	1.42	0.25	74.54	17.7+/-21.2	13.63+/-1.95 (5)	before 8-2	before 12-5	poor - not included in Fig. 2
05JBBL071	EC2	38	1.43	0.3	49.12	40.3+/-5.0	12.18+/-2.64 (49)	45-42	41-25	good - included in Fig. 2
05JBBL067	*EC3*	*38*	*1.54*	*0.29*	*0*	*43.0+/-4.8*	11.59+/-2.65 (38)	55-40	54-45	good - included in Fig. 2
05JBBL065	*EC6*	*39*	*1.51*	*0.29*	*0.01*	*57.1+/-7.8*	*12.57+/-2.57 (193)*	60-35	45-35	good - included in Fig. 2
05JBBL064	EC7	37	1.48	0.27	6.1	20.7+/-4.2	14.13+/-1.72 (122)	25-15	23-19	good - included in Fig. 2; see also Fig. DR2
05JBBL064z	EC7	20	NA	NA	0	604+/-56	NA	NA	NA	NA
05JBBL062	*EC8*	*5*	*1.43*	*0.28*	*0*	*7.3+/-4.8*	14.73+/-1.07 (9)	14-5	11-5	poor - not included in Fig. 2
							Interandean zone			
05JBBL060	IA1	2	1.29	0.24	92.06	0.5+/-1.0	15.23+/-2.63 (5)	5-2	no fits	poor - not included in Fig. 2
05JBBL059	IA2	19	1.69	0.41	84.65	126 +/-100	10.45+/-2.39 (90)	30-2	18-2	good - included in Fig. 2; see also Fig. DR2
05JBBL058	*IA3*	*27*	*1.39*	*0.24*	*0*	*8.1+/-3.6*	*14.03+/-1.81 (28)*	13-6	13-6	good - included in Fig. 2
							Subandes			
05JBBL056	SA1	32	1.33	0.24	65.13	5.6+/-2.0	14.16+/-1.54 (40)	7-4	7-5	good - included in Fig. 2; see also Fig. DR2
05JBBL055	SA2	34	1.44	0.24	35.54	4.1+/-1.4	14.22+/-1.41 (33)	6-3	~5	good - included in Fig. 2; see also Fig. DR2
05JBBL054	SA3	14	1.53	0.34	100	1.8+/-2.6	14.27+/-1.2 (23)	6-2	5-3	good - included in Fig. 2; see also Fig. DR2
05JBBL052	*SA4*	*30*	*1.43*	*0.27*	*0.02*	*3.0+/-1.4*	14.15+/-1.12 (44)	no fits	no fits	good, but no model fits

Sample #	ID	n	Dpar µm	Dper µm	P (χ^2) %	Pooled Age Ma ± 2σ	MTL ± 1σ (N_t) µm (trks)			
							Altiplano			
B815-5	*AL1*	*13*	*1.76*	*0.46*	*0.1*	*83.5±20.8*	*12.03±2.26 (51)*	60-20	50-25	good - but AL not included in Fig. 2 (see caption)
B815-1	AL2	24	1.62	0.44	59.2	43.2±13.6	12.43±2.16 (100)	56-38	45-27	good - but AL not included in Fig. 2 (see caption)
							Eastern Cordillera			
B611-5	*EC4*	*37*	*1.77*	*0.44*	*0*	*68.9±9.8*	*11.9±2.11 (201)*	32-18	22-14	good - included in Fig. 2
66-7	EC5	31	1.68	0.48	59.8	28.0±5.6	12.59±1.79 (121)	33-26	33-30	good - included in Fig. 2; see also Fig. DR2

First 8 columns are from Table DR2.

Range for onset time of rapid cooling from HeFTy thermal modeling is reported for both acceptable and good fits; good fits highlighted in text.

Poor data not shown on Fig. 3 in main text

NA = not applicable

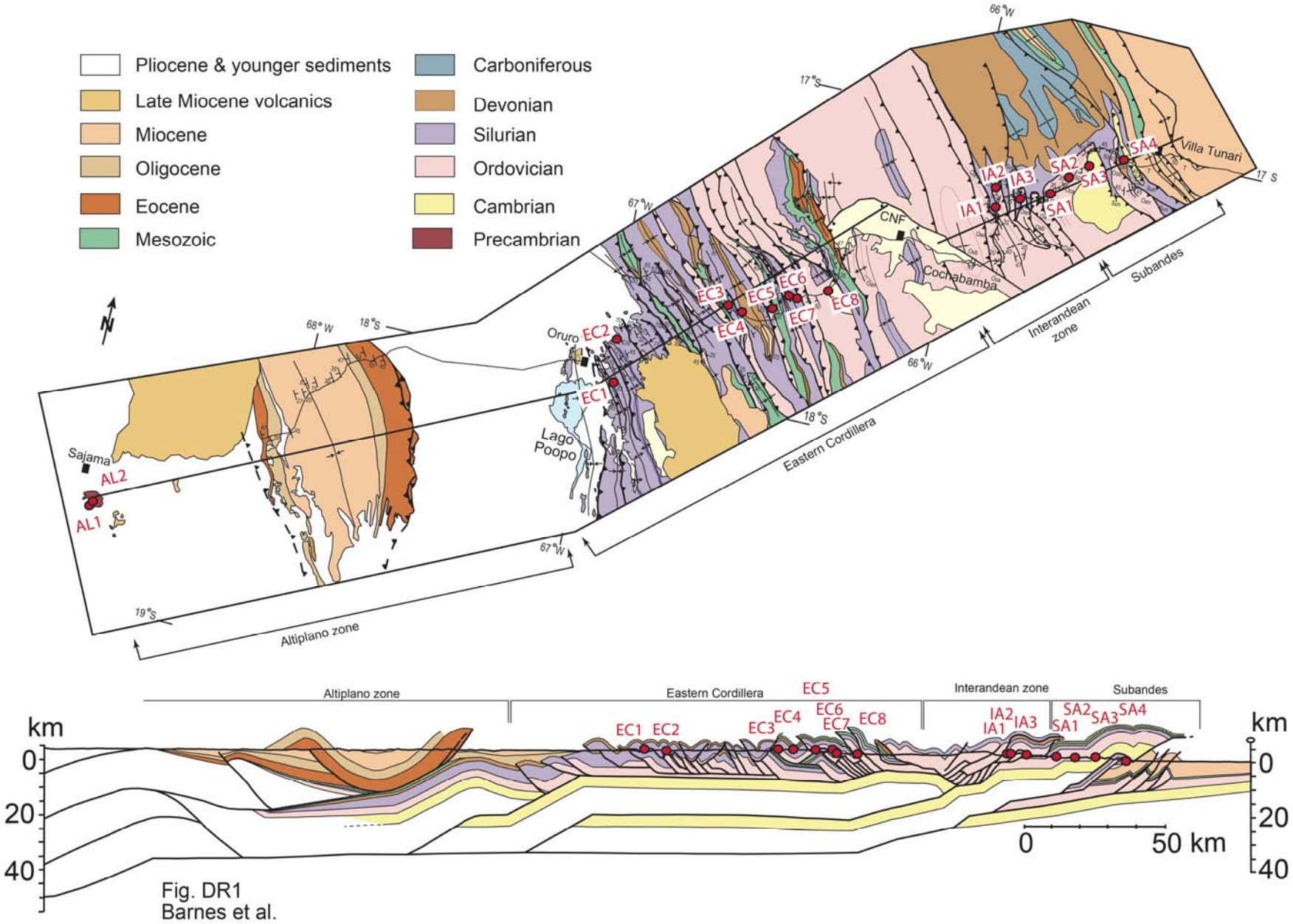

Figure DR1. Geologic map and cross section along the central transect (simplified from McQuarrie, 2002). Red dots and text are sample locations/IDs of the new fission track data (Table DR2) presented in this paper.

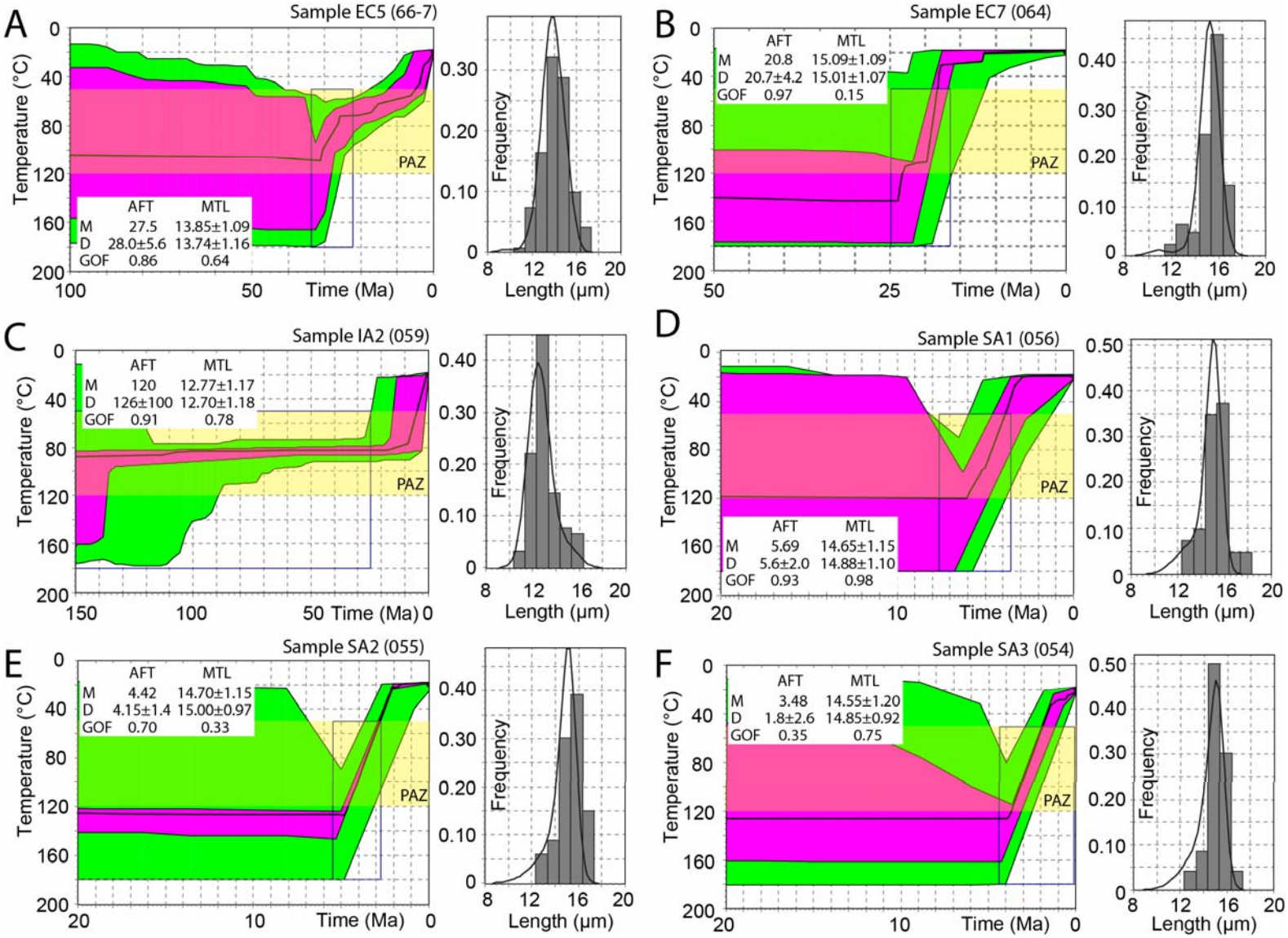

Figure DR2. Example thermal histories from the central AFT data from west to east (A-F). HeFTy (Ketcham, 2005) thermal modeling showing permissible temperature-time (T-t) histories (left diagrams) and measured vs. modeled length distributions (right diagrams: histograms measured data, best-fit model is the curve). Green areas are acceptable fits, pink areas are good fits, the black line is the best fit, and imposed model constraints are the boxes. Pooled apatite ages (AFT), mean track lengths (MTL), and goodness of fit (GOF) between the model (M) results and the data (D) are tabulated. Modeled T-t paths are only well constrained within the partial annealing zone (PAZ: yellow band).

REFERENCES

Barnes, J. B., Ehlers, T. A., McQuarrie, N., O'Sullivan, P. B., and Pelletier, J. D., 2006, Variations in Eocene to recent erosion across the central Andean fold-thrust belt, northern Bolivia: Implications for plateau evolution: Earth and Planetary Science Letters, v. 248, p. 118-133.

Barnes, J. B., Ehlers, T. A., McQuarrie, N., O'Sullivan, P. B., and Tawackoli, S., 2008, Thermochronometer record of central Andean Plateau growth, Bolivia (19.5ºS): Tectonics, v. 27, TC3003, doi:3010.1029/2007TC002174.

Donelick, R. A., O'Sullivan, P. B., and Ketcham, R. A., 2005, Apatite Fission-Track Analysis, *in* Reiners, P. W., and Ehlers, T. A., eds., Low-Temperature Thermochronology: Techniques, Interpretations, and Applications, p. 49-94.

Ege, H., Sobel, E. R., Scheuber, E., and Jacobshagen, V., 2007, Exhumation history of the southern Altiplano plateau (southern Bolivia) constrained by apatite fission-track thermochronology: Tectonics, v. 26, TC1004, doi:1010.1029/2005TC001869.

Ehlers, T. A., Chaudhri, T., Kumar, S., Fuller, C. W., Willett, S. D., Ketcham, R. A., Brandon, M. T., Belton, D. X., Kohn, B. P., Gleadow, A. J. W., Dunai, T. J., and Fu, F. Q., 2005, Computational tools for low-temperature thermochronometer interpretation, *in* Reiners, P. W., and Ehlers, T. A., eds., Low-Temperature Thermochronology: Techniques, Interpretations, and Applications, p. 589-622.

Henry, S. G., and Pollack, H. N., 1988, Terrestrial heat flow above the Andean subduction zone in Bolivia and Peru: Journal of Geophysical Research, v. 93, p. 15153-15162.

Insel, N., Poulsen, C. J., Ehlers, T. A., and Sturm, C., 2012, Response of meteroic $\delta^{18}O$ to surface uplift - Implications for Cenozoic Andean Plateau growth: Earth and Planetary Science Letters, v. 317-318, p. 262-272.

Ketcham, R. A., 2005, Forward and inverse modeling of low-temperature thermochronometry data, *in* Reiners, P. W., and Ehlers, T. A., eds., Low-Temperature Thermochronology: Techniques, Interpretations, and Applications, p. 275-314.

Ketcham Ketcham, R. A., Carter, A. C., Donelick, R. A., Barbarand, J., and Hurford, A. J., 2007, Improved modeling of fission-track annealing in apatite: American Mineralogist, v. 92, p. 799-810.

McQuarrie, N., 2002, The kinematic history of the central Andean fold-thrust belt, Bolivia: implications for building a high plateau: Geological Society of America Bulletin, v. 114, p. 950-963.

Springer, M., 1999, Interpretation of heat-flow density in the Central Andes: Tectonophysics, v. 306, p. 377-395.

Springer, M., and Forster, A., 1998, Heat-flow density across the Central Andean subduction zone: Tectonophysics, v. 291, p. 123-139.